Phase Behavior of Semiflexible Diblock Copolymers

Chandralekha Singh[†] and Mark Goulian[‡]

Department of Physics, University of California, Santa Barbara, California 93106

Andrea J. Liu[§] and Glenn H. Fredrickson[*]

Department of Chemical and Nuclear Engineering, University of California, Santa Barbara, California 93106

Received October 22, 1993; Revised Manuscript Received February 19, 1994[⊗]

ABSTRACT: We examine the phase behavior of diblock copolymers of arbitrary flexibility near their order–disorder transition. Our approach is based on a free energy functional calculated from a microscopic model of rigid rods connected with free joints and depends only on a small set of parameters, including the Flory χ parameter, a Maier–Saupe parameter, and the rod lengths and molecular weights of each block. By analyzing spinodals within this model, we have explored the effect of differences in flexibility between the two blocks, as well as the stiffness of the diblock as a whole, on the phase behavior. We find that nematic and microphase fluctuations can significantly affect transition temperatures and phase boundaries when the difference in stiffness is large.

I. Introduction

A diblock copolymer is a polymer consisting of a sequence (or block) of one type of monomer, A, joined chemically to a block of another type of monomer, B. At high temperatures, a melt of diblocks tends to mix into an isotropic, disordered phase with uniform composition. At low temperatures, diblocks cannot phase separate on a macroscopic scale because the A and B blocks are joined together. Instead, they tend to demix into microphases, characterized by alternating regions rich in each block. Microphase separation of flexible diblocks has been studied extensively for more than a decade,[1] but the thermodynamics of semiflexible diblocks have received only recent attention. In this paper, we focus on the effect of differences in flexibility between the two blocks, as well as the effect of increased stiffness of the diblock as a whole, on the order–disorder transition. Differences in flexibility affect miscibility in polymer blends[2-4] as well as interfacial tensions[5,6] and should therefore strongly influence miscibility in diblock copolymers. Moreover, if the diblock is sufficiently stiff, liquid crystalline phases such as nematic and smectic C phases might be observable in addition to the smectic A (lamellar) phase typically formed by flexible diblocks.

Microphase-separated block copolymers with blocks of different stiffnesses are technologically useful as polymeric composites. The flexible blocks provide toughness, or resistance to fracture, while the stiff blocks provide tensile strength and thermal stability.[7-9] In addition, there is considerable interest in developing block copolymers with flexible and conducting polymer blocks. Conjugated polymers tend to be quite stiff due to electronic delocalization. Several groups, including Enkelman, Muller, and Wegner,[10] Chien and co-workers,[11] and Bake and Bates,[12] have synthesized flexible/conjugated multiblock copolymers. Stowell and co-workers[13] reviewed work up to 1988 on block and graft copolymers containing polyacetylene. More recently, Krouse and Schrock[14] and Saunders, Cohen, and Schrock[15] have synthesized flexible/conjugated diblock copolymers.

Another example of a semiflexible diblock is a rigid-rod-like mesogenic block coupled to a flexible block, known as a rodcoil copolymer. Radzilowski, Wu, and Stupp[16] have synthesized such diblocks with polyisoprene as the flexible block and nitroazobenzene coupled to rigid biphenyldicarboxylic acid as the stiff block. Although they observe microphase separation and see nanoscale nematic domains in the microstructure, details of the morphology of the periodic structure, the orientation of the rodlike segments relative to the plane of the thin film, and the exact temperature of the order–disorder transition have not yet been fully explored.

Finally, Almdal and co-workers[17] have studied a less extreme case of semiflexible diblocks where both blocks are flexible polyolefins but have different statistical segment lengths. In this and subsequent work,[2,18] they observe that the phase behavior is profoundly altered by the difference in statistical segment length.

A decade ago, Leibler[19] put forward a Landau–Ginzburg theory to describe the phase behavior of flexible diblocks with equal statistical segment lengths in the limiting regime known as the weak segregation limit (WSL), where interactions between the blocks are sufficiently weak so that individual chain statistics are unperturbed. Leibler's theory, together with subsequent work by Fredrickson and Helfand[20] to include fluctuation effects, has been extremely successful in describing the phase diagram near the order–disorder transition as a function of only a few relevant parameters, namely, the Flory χ parameter, the chain length N, and the fraction of type A monomers, f. In the opposite limiting regime, called the strong segregation limit (SSL), the interaction between the two blocks is sufficiently large so that nearly pure A and B microdomains are separated by narrow interfaces. The SSL has been studied by several groups for flexible diblocks. Helfand and Wasserman[21] developed a self-consistent field theory that allows quantitative calculations of free energies, composition profiles, and chain conformations. Their numerical calculations of phase diagrams in the SSL are in good agreement with experimental results. Semenov[22] developed an analytical technique for the $\chi N \to \infty$ limit, which was later extended by Milner, Witten, and Cates,[23] where the strongly stretched nature of the copolymers was

* To whom correspondence should be addressed.
[†] Current address: Department of Materials Science & Engineering, University of Illinois, Urbana, IL 61801.
[‡] Current address: Exxon Research & Engineering Co., Annandale, NJ 08801.
[§] Permanent address: Department of Chemistry & Biochemistry, UCLA, Los Angeles, CA 90024.
[⊗] Abstract published in *Advance ACS Abstracts*, April 1, 1994.

0024-9297/94/2227-2974$04.50/0

exploited to approximate the configurational integrals by the classical extremum of the energy functional. Finally, we note that Ohta and Kawasaki[24] used a free energy functional derived from the random phase approximation (RPA), not strictly valid in the SSL, to obtain results qualitatively similar to those of Helfand and Semenov.

Vavasour and Whitmore[25] generalized the self-consistent mean field theory for flexible diblock copolymers to include different statistical segment lengths for each block. Their numerical results, however, were confined to the case of equal statistical segment lengths.

The effect of block flexibility on the isotropic–nematic transition has been studied by two groups. Fredrickson and Leibler[35] considered a melt of random copolymers made up of two monomers that have different flexibilities. They found that the system separates on a macroscopic scale at the isotropic–nematic transition into a nematic phase of copolymers with a higher fraction of the stiffer monomer, coexisting with an isotropic phase of copolymers with a higher fraction of the more flexible monomer. Wang and Warner[27] examined a melt of multiblock copolymers made up of alternating rod and coil blocks and calculated the decrease of the isotropic–nematic transition temperature with increasing molecular weight of the coil block.

Microphase separation in a melt of rodcoil diblocks was first studied theoretically by Semenov and Vasilenko.[28] They found that the melt can form a nematic phase for small values of χ when the volume fraction of the rigid block is large. With increasing χ, various smectic phases were predicted, including a monolayer lamellar phase at small χ and a bilayer lamellar phase at large χ. In the monolayer lamellar phase, rod-rich layers with a thickness comparable to the length of the rods alternate with coil-rich layers. In the bilayer lamellar phase, rod-rich layers of twice the length of the rods alternate with coil-rich layers. In the monolayer configuration, the lateral distance between flexible coils is larger than in the bilayer configuration, but the total rod–coil interfacial area is larger. Thus, when the interfacial tension is low (small χ), the system forms monolayer lamellae to reduce the elastic stretching of coils. When the interfacial tension is high (large χ), the system prefers to form bilayer lamellae to reduce the total interfacial area. Halperin[29] and Semenov[30] also predicted a transition from a smectic A to a smectic C phase in diblocks with a large volume fraction of the flexible coil. In the smectic A phase, the rodlike blocks are aligned normal to the layers, while in the smectic C phase, the chains are tilted by some angle relative to the layer normal. In the smectic A phase, the total interfacial area is lower but the lateral distance between coils is smaller so the elastic energy cost is higher; in the smectic C phase, the elastic energy is lower but the interfacial energy is higher. Williams and Fredrickson[31] suggested yet another possibility when the volume fraction of coils is high, namely, the "hockey puck" phase. This is a discrete micellar phase where rods are packed axially into cylinders. Williams and Fredrickson argued that this microstructure enables the chains grafted to the top and bottom surfaces of the cylinders to fan out, thus reducing the elastic energy of the coils at the cost of creating an extra curved surface. Finally, Williams and Halperin[32] recently examined the phase diagrams of semiflexible–flexible chain diblocks. They assume that the isotropic–nematic transition occurs when the system is already in the SSL and study the competition between lamellar, cylindrical, and spherical microphase structures. Since their analysis assumes that the semiflexible chain elasticity is controlled by hairpin defects, it only applies to high molecular weight blocks.

The first study of the thermodynamics of rodcoil diblock copolymer melts in the WSL was done by Holyst and Schick.[33] They calculated the Landau expansion in two order parameters, the composition order parameter employed by Leibler[19] and an orientational density order parameter. This second order parameter is needed when individual monomers have a rigid, anisotropic character and describes transitions to orientationally ordered phases such as nematics. Similar two-order-parameter theories have proved quite useful in the study of binary blends of rods and coils[34] or of polymers of arbitrary stiffness.[4,35] Holyst and Schick[33] calculated the expansion coefficients of the Landau theory up to second order using the random phase approximation, starting with a microscopic model of rodcoil chains with a Gaussian block joined to a rigid rod block. Interactions were included through a Flory interaction parameter to describe isotropic interactions and a Maier–Saupe parameter to describe anisotropic interactions. Holyst and Schick showed that the lamellar domain boundaries are sharper for longer rods. They also studied the phase behavior of the rodcoil melt as a function of the interaction parameters.

Our study of the phase behavior of semiflexible diblocks is in the same spirit as Holyst and Schick's. We also use the random phase approximation to calculate the Landau–Ginzburg free energy functional up to second order in composition and orientational density order parameters. Unlike Holyst and Schick, however, we have formulated the free energy for blocks with arbitrary flexibility. This enables us to study phase behavior as a function of global and individual block flexibilities. In our microscopic model, one block is composed of N_A rigid rods of length $b_A a_0$ connected by free joints, while the other block is composed of N_B rigid rods of length $b_B a_0$, where the monomer length a_0 is the same for both species. Our free energy functional therefore depends on a small set of parameters, namely, the number and length of rods in each block, the isotropic interaction parameter χ, and the anisotropic interaction parameter w. It should also be noted that no gradient expansion is involved; hence, the vertex functions in the free energy are also complicated functions of the wave vector of the microphase pattern. Since we have expanded the free energy to quadratic order in the two order parameters about the isotropic phase, we can only study the spinodals from the isotropic phase—that is, we can study transitions from the isotropic phase to the nematic phase, or from the isotropic to the microphase region, but we cannot examine transitions among the different microphases or transitions from the nematic phase to any of the microphases.

II. Microscopic Model and Free Energy Functional

An example of our microscopic model of diblocks is shown in Figure 1. Both species A and B are composed of rigid cylindrical segments, or monomers, of fixed length a_0, diameter $d_0 = a_0(4/\pi)^{1/2}$, and volume $v_0 = a_0^3$. The A block is composed of N_A rigid rods connected by free joints; each rod contains b_A segments. Similarly, the B block is composed of N_B rods, each containing b_B monomers. Thus, the persistence lengths of the blocks are $b_A a_0$ and $b_B a_0$, the contour lengths of the blocks are $N_A b_A a_0$ and $N_B b_B a_0$, and the contour length of the entire copolymer is $Na_0 = N_A b_A a_0 + N_B b_B a_0$. We consider only incompressible melts[36] of monodisperse semiflexible diblock copolymers, so the volume fraction of A is

$$f = N_A b_A/(N_A b_A + N_B b_B) \tag{2.1}$$

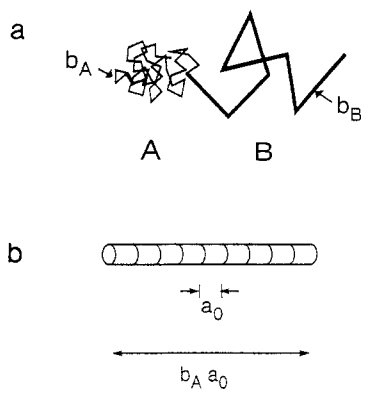

Figure 1. (a) Microscopic model of diblocks showing the A block (thin lines) composed of N_A rigid rods, each with b_A monomers, and the B block (heavy lines) composed of N_B rigid rods of b_B monomers each. The rigid rods are connected by free joints. Individual monomer segments are not shown. (b) Representation of a type-A rigid rod as b_A contiguous cylindrical segments, each of length a_0.

To characterize the various phases of semiflexible copolymers, we introduce two microscopic order parameters for each block. One of these is the standard composition order parameter, which describes the deviation of the local volume fraction of a species from the average global volume fraction. Thus, we define the order parameters

$$\hat{\phi}_A(\vec{r}) = \hat{\varphi}_A(\vec{r}) - f$$
$$\hat{\phi}_B(\vec{r}) = \hat{\varphi}_B(\vec{r}) - (1-f) \tag{2.2}$$

where $\hat{\varphi}_A$ and $\hat{\varphi}_B$ are the local volume fractions of A and B, respectively:

$$\hat{\varphi}_A(\vec{r}) = v_0 \sum_m \sum_{n=1}^{N_A} \int_{-b_A/2}^{b_A/2} ds\ \delta[\vec{r} - (\vec{r}_{n,m} + s\vec{u}_{n,m})]$$
$$\hat{\varphi}_B(\vec{r}) = v_0 \sum_m \sum_{n=1}^{N_B} \int_{-b_B/2}^{b_B/2} ds\ \delta[\vec{r} - (\vec{r}_{n,m} + s\vec{u}_{n,m})] \tag{2.3}$$

Here, the variable m indexes different copolymer chains, while n runs over rods in a given block and s runs over monomers in a given rod. (Our notation for the variable s suggests a continuum limit that will be applied throughout.) We define $\vec{r}_{n,m}$ as the center-of-mass position and $\vec{u}_{n,m}$ as the tangent vector of rod n of chain m; thus, the position vector of segment s on rod n of chain m is $\vec{r}_{n,m} + s\vec{u}_{n,m}$. Since the monomer segments are rigid, we constrain the length of the tangent vector to be unity for all segments. Note that the thermal average of $\hat{\varphi}_A(\vec{r})$ is simply f in the disordered phase, so the thermal average of $\hat{\phi}_A(\vec{r})$ vanishes in the disordered phase.

The second order parameter introduced for each species is the local nematic tensor order parameter. This describes orientational order. The nematic order parameters for species A and B are

$$\hat{S}_A^{ij}(\vec{r}) = \sum_m \sum_{n=1}^{N_A} \int_{-b_A/2}^{b_A/2} ds\ \delta[\vec{r} - (\vec{r}_{n,m} + s\vec{u}_{n,m})]\left[u_{n,m}^i u_{n,m}^j - \frac{1}{3}\delta^{ij}\right]$$

$$\hat{S}_B^{ij}(\vec{r}) = \sum_m \sum_{n=1}^{N_B} \int_{-b_B/2}^{b_B/2} ds\ \delta[\vec{r} - (\vec{r}_{n,m} + s\vec{u}_{n,m})]\left[u_{n,m}^i u_{n,m}^j - \frac{1}{3}\delta^{ij}\right] \tag{2.4}$$

Note that in the isotropic phase, the thermal averages of $\hat{S}_A^{ij}$ and $\hat{S}_B^{ij}$ are zero.

As stated earlier, the enthalpic contributions to the free energy are characterized by two pairwise interaction parameters, namely, the standard Flory interaction parameter χ and the Maier–Saupe parameter w. These interaction parameters could arise from enthalpic or from steric excluded volume interactions.[37] We describe the isotropic interactions between segments A–A by χ_{AA}, between B–B by χ_{BB}, and between A–B by χ_{AB}. For an incompressible melt, we define a single effective interaction parameter $\chi = \chi_{AB} - (\chi_{AA} + \chi_{BB})/2$. Similarly, we define the anisotropic interactions w_A, w_B, and w_{AB} between A–A, B–B, and A–B monomers, respectively. These anisotropic interactions favor parallel alignment of segments when they are positive in sign. To minimize the number of interaction parameters, we assume that all of the Maier–Saupe parameters are the same: $w = w_A = w_B = w_{AB}$. This simplifies the analysis without qualitatively changing our general results. In principle, the parameter χ can be varied through zero; the parameter w, on the other hand, is always nonzero due to excluded volume interactions. Thus it would seem that the ratio of anisotropic interaction strength to isotropic interaction strength w/χ can be arbitrarily large. In practice, however, χ is positive when the two species have different stiffnesses. Indeed, a difference in stiffness alone apparently gives rise to a positive entropic contribution to χ,[40] so we anticipate that physical values of the ratio w/χ will lie within an order of magnitude of unity.

The calculation of the Landau–Ginzburg expansion coefficients to quadratic order is similar to calculations presented in section III of Leibler's paper[19] and by Holyst and Schick.[33] Since Leibler was interested in flexible diblocks, he retained only the composition order parameter. Holyst and Schick studied rodcoil diblocks, so they retained the composition and the orientation of the rod component as two order parameters. We are interested in diblocks of arbitrary flexibility, so we have retained the composition of one component and the orientation of both components as three separate order parameters. We compute various noninteracting pair correlation functions of the order parameters at all wave vectors k (see Appendix A). We then perform a Legendre transformation by inverting the matrix consisting of the correlation functions (see Appendix B).

The Landau–Ginzburg free energy F is conveniently written as a dimensionless free energy per monomer $\mathcal{F}$

$$\mathcal{F}[\phi, \overleftrightarrow{S}_A, \overleftrightarrow{S}_B] = \beta F[\phi, \overleftrightarrow{S}_A, \overleftrightarrow{S}_B] v_0/V \tag{2.5}$$

where ϕ is the thermal average $\hat{\phi}_A$ (because of incompressibility, $\phi_A(\mathbf{k}) = -\phi_B(\mathbf{k})$), and $\overleftrightarrow{S}_A$ and $\overleftrightarrow{S}_B$ are the thermal averages of $\hat{\overleftrightarrow{S}}_A$ and $\hat{\overleftrightarrow{S}}_B$, respectively. Note that since S_A^{ij} and S_B^{ij} are irreducible second-rank tensors describing uniaxial nematic order, they must have the following form in reciprocal space:

$$S_A^{ij}(\mathbf{k}) = S_A(\mathbf{k})\left(n_i^A n_j^A - \frac{1}{3}\delta^{ij}\right)$$

$$S_B^{ij}(\mathbf{k}) = S_B(\mathbf{k})\left(n_i^B n_j^B - \frac{1}{3}\delta^{ij}\right) \tag{2.6}$$

where $\hat{n}^A(\mathbf{k})$ and $\hat{n}^B(\mathbf{k})$ are unit directors for species A and B.

In reciprocal space, we obtain

$$\begin{aligned}\mathcal{F} = \frac{1}{2}\sum_{\mathbf{k}}[A(\mathbf{k}) - 2\chi]\phi(\mathbf{k})\,\phi(-\mathbf{k}) + [B_A(\mathbf{k}) - w_A]S_A(\mathbf{k})\,S_A(-\mathbf{k}) + [B_B(\mathbf{k}) - w_B]S_B(\mathbf{k})\,S_B(-\mathbf{k}) + [B_{AB}(\mathbf{k}) - w_{AB}](S_A(\mathbf{k})\,S_B(-\mathbf{k}) + S_A(-\mathbf{k})\,S_B(\mathbf{k})) + C_A(\mathbf{k})[\phi(\mathbf{k})\,S_A(-\mathbf{k}) + \phi(-\mathbf{k})\,S_A(\mathbf{k})] + C_B(\mathbf{k})[\phi(-\mathbf{k})\,S_B(\mathbf{k}) + \phi(\mathbf{k})\,S_B(-\mathbf{k})]\end{aligned} \tag{2.7}$$

Expressions for $A(\mathbf{k})$, $B_A(\mathbf{k})$, $B_B(\mathbf{k})$, etc. in terms of the noninteracting pair correlation functions are provided in Appendix B. Note that $B_A(\mathbf{k})$, $B_B(\mathbf{k})$, $C_A(\mathbf{k})$, and $C_B(\mathbf{k})$ all depend on the angles between $\mathbf{k}$ and the directors $\hat{n}^A(\mathbf{k})$ and $\hat{n}^B(\mathbf{k})$.

III. Base Set of Equations for Spinodals

To determine the phase diagram, we minimize the free energy with respect to the order parameters and the wave vector $\mathbf{k}$. Since we have expanded the free energy only to quadratic order, the low-temperature behavior is inaccessible to us. Instead, we study the stability limits of the isotropic, disordered phase. At high temperatures (small χ and w), the isotropic phase is stable to perturbations in composition and orientation. At lower temperatures, however, the isotropic phase may become unstable to either the nematic phase or to a microphase. Unfortunately, we are unable to distinguish between the smectic A (lamellar) microphase and other microphases such as the hexagonal phase of cylinders, the bcc phase of spheres, or the hockey puck phase. A higher order calculation of the free energy would be necessary to differentiate between these structures. In the following analysis, we therefore use the generic term "microphase".

The stability limits of the disordered phase are derived by setting to zero the determinant of the matrix of second derivatives of the free energy with respect to the three order parameters:

$$\det\left[\frac{\partial^2\mathcal{F}}{\partial\xi_i(\mathbf{k})\,\partial\xi_j(-\mathbf{k})}\right] = 0 \tag{3.1}$$

where $\vec{\xi} = (\phi, S_A, S_B)$.

For a given set of chain parameters, b_A, b_B, N_A, and N_B, our aim is to find the weakest interaction parameters (highest temperatures) for which the disordered phase is unstable. Expressions for the spinodal values χ_s or w_s as functions of the wave vector $\mathbf{k}$ can then be derived from eq 3.1. Finally, we find the minima of χ_s or w_s as functions of $\mathbf{k}$ to obtain the stability limits. If the magnitude k^* at the minimum is nonzero, then the disordered phase is unstable to a microphase, and if the value of k^* is zero, then the disordered phase is unstable to a nematic phase. Note that if there are two equal minima, one at $k^* = 0$ and one at $k^* \neq 0$, then the isotropic phase is unstable to both the nematic phase and a microphase; we call this a triple point.[38]

In carrying out the analysis outlined above, we have also made another approximation. In general, the directors $\hat{n}^A$ and $\hat{n}^B$ defined in eq 2.6 may lie at arbitrary angles θ^A and θ^B relative to $\mathbf{k}$. In the analyses presented in the following sections, however, we have made the simplifying assumption that $\theta^A = \theta^B = 0$ at the minimum of χ_s or w_s with respect to $\mathbf{k}$. If we assume that the microphase is smectic, this corresponds to the smectic A phase. Similarly, $\theta^A \neq 0$ or $\theta^B \neq 0$ corresponds to the smectic C phase. For f near 0.5, we expect, on the basis of arguments by Halperin[29] and Semenov,[30] that the smectic A phase should preclude the smectic C phase at the transition from the isotropic phase. At compositions near $f = 0$ or $f = 1$, we expect ordered micellar phases to preempt the smectic C phase. We have performed the general analysis, minimizing χ_s or w_s with respect to $k = |\mathbf{k}|$, θ^A, and θ^B, for some special cases and have always found that the minimum lies at $\theta^A = \theta^B = 0$. Since it is probable that the smectic C phase is always precluded by some other phase near the isotropic phase, we are justified in neglecting it in our spinodal analysis.

The equation of χ_s that satisfies eq 3.1 is the same equation that we obtain by first integrating the free energy over $\overleftrightarrow{S}_A$ and $\overleftrightarrow{S}_B$ and then taking the second derivative with respect to ϕ, because our theory is quadratic in those order parameters. Thus, the spinodal value of χ is also the effective value of χ once orientational degrees of freedom have been integrated out. This effective χ hence contains contributions from orientational fluctuations. Similarly, the equation for w_s that satisfies eq 3.1 is the same one that would be obtained by integrating over ϕ. Therefore, by solving eq 3.1 for the spinodal value of w, we have included compositional, or microphase, fluctuations at the Gaussian level.

IV. Results

We have constructed phase diagrams as a function of varying chain stiffness. Our aim is to describe trends as the difference in stiffnesses between the two blocks is varied and as the stiffness of the diblock as a whole is increased. In particular, we are interested in the spinodal value of the Flory χ parameter for fixed Maier–Saupe parameter w, and the spinodal value of w for fixed χ, as well as k^*, the preferred wave vector of the microphase, as functions of chain stiffness and volume fraction f. To this end, we have studied several different series of diblock copolymers. Within each series, the total number of monomers $N = N_A b_A + N_B b_B$ is held fixed while N_A, b_A, N_B, or b_B is varied. We have studied the dependence of χ on N separately in each case and find that for chain lengths exceeding roughly 10 times the persistence length of the stiffer block, *i.e.*, for $N \gtrsim 10 b_B$, for $b_B > b_A$, χ varies inversely with N, as expected.

A. Series I: Flexible–Semiflexible Diblocks. In series I, we start with a flexible diblock melt, similar to that studied by Leibler. The volume fraction f, defined in eq 2.1, is held fixed at $f = 0.5$. We begin with $b_A = 1$, $b_B = 1$, $N_A = N/2$, and $N_B = N/2$. In this case, we fix $N = 200$. We then increase the persistence length b_B of the B block, keeping $b_A = 1$ fixed. Note that N_B must correspondingly decrease since f is fixed. Series I therefore consists of a family of diblocks where the A block is always a flexible coil and the B block ranges from a flexible coil to a rigid rod. Note that the smectic A phase is the stable microphase and the transition from the isotropic phase is most weakly first order at $f = 0.5$ for the symmetric limit $b_A = b_B = 1$, so our analysis is more relevant to the true phase behavior when the B block is a flexible coil than when it is a rigid rod.

In the first set of calculations on series I, we fix the strength of the anisotropic interaction parameter w. In Figure 2a, we plot the spinodal value $\chi_s N$ as a function of b_B/N for $w = 0$ (solid), $w = 0.2$ (dashed), and $w = 0.75$ (dotted) as the B block is varied from a flexible coil (b_B/N

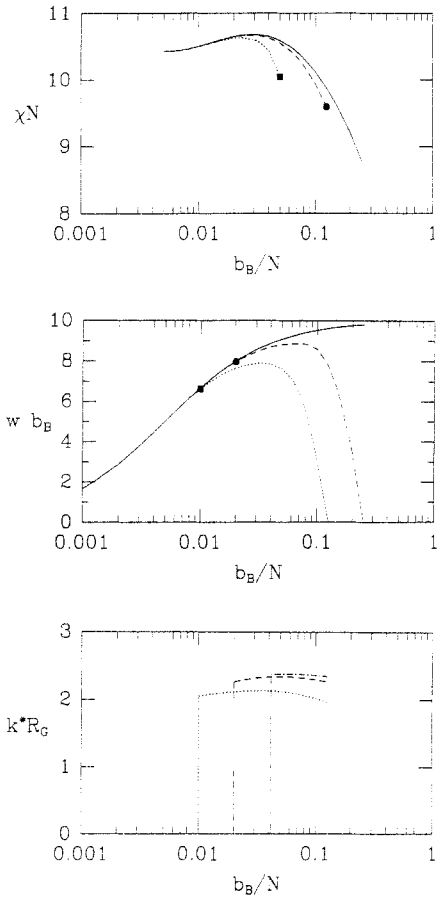

Figure 2. Phase diagrams for series I (flexible–semiflexible diblocks) with $N = 200$, $b_A = 1$, and $N_A = 100$. The B block is varied from $b_B = 1$ to $b_B = 100$, with $N_B = 100/b_B$. (a, Top) The spinodal value of χN *vs* b_B/N for $w = 0$ (solid), $w = 0.2$ (dashed), and $w = 0.75$ (dotted). These curves represent the transition from the isotropic to the smectic phase. The large solid circle and square at the end of the dashed and dotted curves, respectively, mark the triple point, where the isotropic, nematic, and smectic phases coexist. (b, Middle) The spinodal value of wb_B *vs* b_B/N for $\chi N = 0$ (solid), $\chi N = 9.0$ (dashed), and $\chi N = 10.0$ (dotted). The solid curve represents the transition from the isotropic phase to the nematic phase at $\chi = 0$. The dashed and dotted curves mark the isotropic–nematic transition to the left of the large solid circle and square, respectively, and mark the isotropic–smectic transition to the right of the solid symbols. (c, Bottom) The wave vector k^*R_g of the ordered phase in units of the radius of gyration *vs* b_B/N for $\chi N = 8.5$ (dot–dashed), $\chi N = 9.0$ (dashed), and $\chi N = 10.0$ (dotted). In the nematic phase, $k^*R_g = 0$ and in the smectic phase, $k^*R_g > 0$. Note that the onset of the smectic phase moves to smaller b_B as χ increases.

$= 1/N$) to a rod ($b_B/N = 1/2$). The spinodal value χ_s is our best estimate, within the quadratic theory, of the position of the order–disorder transition. Thus, when χ is smaller than the spinodal value, we predict the system is in the disordered phase, and when χ exceeds the spinodal value, we predict the system is in a microphase (where $k^* > 0$). Note that in the flexible limit, where $b_B/N \ll 1$, $\chi_s N$ approaches 10.5, in agreement with the value predicted by Leibler for flexible diblocks.[19] From Leibler's analysis, we also know that the microphase is a smectic A phase there. As b_B increases, $\chi_s N$ first increases, until b_B is of the order of the radius of gyration of the flexible A block, and then decreases. We remark that the actual numerical change in $\chi_s N$ with stiffness is disappointingly small, although the trends are interesting. The initial increase of $\chi_s N$ implies that at $f = 0.5$, the blocks initially become more miscible as b_B increases. This is consistent with phase diagrams that will be discussed later (Figure 6), where the spinodal curve shifts to higher volume fractions of the stiffer component. This may be understood in terms of the spontaneous curvature of the copolymer layers that compose the smectic structure. When $f = 0.5$ and $b_B > b_A$, there is a spontaneous curvature in the ordered phase that favors the stiffer component on the inside, since it costs less entropy to stretch stiffer chains. The presence of spontaneous curvature makes the smectic phase less favorable, so a stronger interaction χ is required to drive the system from a disordered to a smectic phase. This is why $\chi_s N$ initially increases with b_B/N in Figure 2a. It must be noted, however, that experiments by Bates and co-workers[2] on the order–disorder transition in diblock copolymer melts show the opposite trend. They find that as b_B increases, a weaker interaction χ is required to drive the system into the ordered phase. Recently, Bates and Fredrickson showed that there is a contribution to χ arising from short-wavelength fluctuations that favors phase separation in homopolymer blends.[40] This contribution, which is not included in our calculation, should affect microphase separation at scales on the order of the radius of gyration as well and may exceed the shift in χ_s due to spontaneous curvature effects that we find here.

As the B block stiffens, it costs less conformational entropy to induce a nonzero orientational density $\overleftrightarrow{S}$. In the simplest case of a smectic phase, there is a nonzero $\overleftrightarrow{S}$ because the chains are stretched parallel to $\vec{k}^*$ (in the direction of translational order). So as the B block stiffens, it costs less conformational entropy to form the smectic phase, and therefore a smaller χ is required to drive the system from the isotropic to the smectic phase. Thus, for small b_B/b_A, our results show that $\chi_s N$ increases in Figure 2a due to spontaneous curvature effects, but for large b_B/b_A, $\chi_s N$ decreases because the conformational entropy cost of the smectic phase decreases. In the extreme case of a rodcoil diblock $b_B/N = 1/2$, our results are consistent with those of Holyst and Schick.[33]

We now turn to the dependence of χ on w, shown in Figure 2a as the differences between the solid curve ($w = 0$), the dashed curve ($w = 0.2$), and the dotted curve ($w = 0.75$). We find that $\chi_s N$ decreases as w increases. This is expected, since as w increases, it aligns the stiff blocks more effectively. The flexible blocks then prefer to demix from stiffer blocks, in order to increase their conformational entropy. Note that for small b_B, χ_s is quite insensitive to w; this is because the difference in stiffness is still small. Finally, for very large b_B and sufficiently large w, we find that the nematic phase actually precludes the microphase. That is, the disordered phase is unstable to the nematic phase rather than to a microphase for sufficiently large b_B. The value of $\chi_s N$ at the onset of the nematic phase is shown in Figure 2a by a large solid symbol (a circle for $w = 0.2$ and a square for $w = 0.75$) at the end of the curve. At the symbol, the isotropic, microphase, and nematic phases coexist, so the solid symbol represents a triple point.[38] Note that the triple point occurs at smaller b_B as w increases, as expected. We have not plotted χ_s beyond the onset of the nematic phase, because the instability to the nematic phase is governed solely by w and is independent of χ at the present level of approximation.

In the second set of calculations on series I, we fix the Flory χ parameter. In Figure 2b, we plot the spinodal value $w_s b_B$ as a function of b_B/N for $\chi N = 0$ (solid), $\chi N = 9.0$ (dashed), and $\chi N = 10.0$ (dotted). For w less than the spinodal value w_s, the system is disordered, and for w greater than the spinodal value, the system is in a nematic phase or microphase. For smaller b_B/N, the three curves in Figure 2b mark the instability of the disordered phase

to the nematic phase, but for larger b_B/N and nonzero χ, the curves represent the instability of the disordered phase to a microphase. The triple points for $\chi N = 9.0$ and $\chi N = 10.0$ are marked by a large solid circle and square, respectively. There is no triple point for $\chi N = 0$. The nematic–microphase boundary is more evident in Figure 2c, where we have plotted k^*R_g (where k^* is the wave vector describing the ordered phase at the transition from the isotropic phase and $R_g = ((N_A b_A^2 + N_B b_B^2)/6)^{1/2}$ is the radius of gyration) as a function of b_B/N for $\chi N = 8.5$ (dot–dashed), $\chi N = 9.0$ (dashed), and $\chi N = 10.0$ (dotted). Note that the dashed and dotted curves in Figure 2c correspond to the same parameters as the dashed and dotted curves in Figure 2b. For small b_B/N, we find from Figure 2c that $k^* = 0$, consistent with the ordered phase being nematic with no translational order. For large b_B/N, however, k^* rises abruptly[39] to a nonzero value, indicating that the ordered phase is now a microphase. From Figure 2c, we see that the microphase preempts the nematic phase at smaller b_B as χ increases. This is expected since χ favors phase separation.

The value of k^* tells us how stretched the chains are in the microphase. In Figure 2c, k^*R_g always lies below 2π in magnitude. This implies that the spacing between lamellae is larger than R_g. The value of k^*R_g predicted by Leibler at the isotropic–smectic transition in the symmetric ($b_A = b_B$, $f = 0.5$) case is $k^*R_g = 1.95$. We find $k^*R_g > 1.95$ when $b_B > b_A$, indicating that the chains are less stretched. This is consistent with experimental results of Bates and co-workers.[18] Note also that as χ increases at fixed b_B, the magnitude of k^*R_g at the smectic spinodal decreases. This is reasonable, since the chains prefer to segregate more as χ increases.

We find that the phase behavior of the extreme case where $N_B = 1$ (rodcoil diblock) is somewhat different from the case where $N_B > 1$, when the B block consists of two or more rods. For example, we find that a slightly larger χ is required for the microphase to preempt the nematic case for $N_B = 1$ than for $N_B = 2$. In general, as discussed in the previous paragraph, the value of χ needed to drive the system into a microphase *increases* as the stiffness decreases, so the rodcoil case violates the trend.

We have chosen the combination wb_B in Figure 2b because we expect $w_s \sim 1/b_B$ when $b_A \ll b_B$ and $\chi = 0$. In general, we expect $w_s \sim 1/(fb_A + (1-f)b_B)$. For fixed $b_A = 1$, this gives the saturation of $w_s b_B$ with large b_B that is shown in the solid curve. When the system is unstable to a microphase (to the right of the solid symbol), we find that $w_s b_B$ decreases rapidly with b_B. In other words, the tendency to demix due to χ is sufficiently strong that only a weak or even negative value of w is required to drive the system from the disordered phase into a microphase. Note also that the magnitude of $w_s b_B$ drops as χ increases at fixed b_B. This is not surprising when the system is unstable to microphase separation. It also occurs when the system is unstable to the nematic phase (left of the solid symbol), although the effect is subtle and not visible in Figure 2b. This effect implies that a weaker anisotropic interaction is required to drive the system from a disordered to a nematic phase when there is a stronger tendency to phase separate. This may be due to microphase fluctuations, which concentrate the stiffer component in regions, making it easier for the stiffer segments to align to form a nematic phase.

The phase behavior implicit in Figure 2a,b is shown explicitly in Figure 3a for a single stiffness $b_B = 50$. (Again, $b_A = 1$, $f = 0.5$, and $N = 200$.) Here we have plotted wb_B as a function of χ/w, the ratio of the isotropic to the anisotropic interaction strength. For small w and χ (high temperatures), the system is in the disordered, isotropic phase, denoted by I. For large w and small χ, the system is in the nematic phase, N. Finally, for large χ, the system exhibits microphase separation, S. There is a triple point, marked by a large dot, where the isotropic, microphase, and nematic phases coexist. The dashed line in Figure 3a shows the nematic spinodal preempted by the microphase. There is a similar microphase spinodal preempted by the nematic phase that is not shown here because it lies extremely close to the isotropic–nematic transition line. The nematic–microphase transition is not shown here because it cannot be calculated within our quadratic Landau theory.

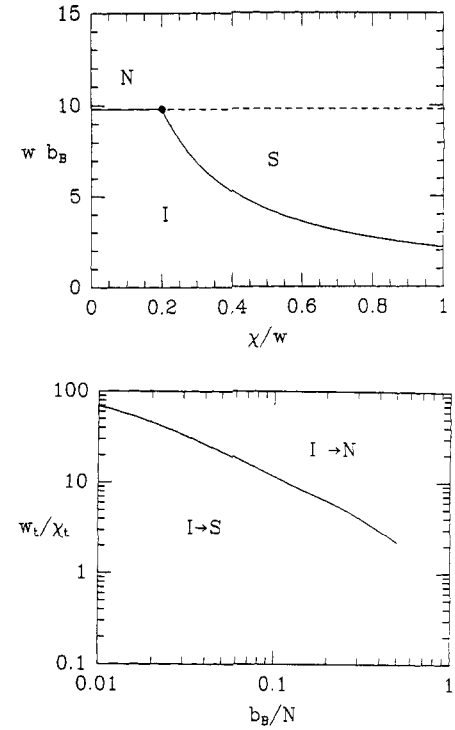

Figure 3. Phase diagrams for series I (flexible–semiflexible diblocks) for the same parameter values as in Figure 2. (a, Top) wb_B *vs* χ/w for fixed $b_B = 50$. The system is in the isotropic phase (I) for low w and χ, the nematic phase (N) for high w, and the smectic phase (S) for high χ. The triple point where the isotropic, nematic, and smectic phases coexist is marked by a large dot. The dashed line represents the instability of the isotropic phase to the nematic phase that is precluded by the I–S transition. The instability of the isotropic phase to the smectic phase that is precluded by the I–N transition lies very close to the I–N transition and is not shown here. The N–S transition cannot be calculated with this free energy, so it is not shown here. (b, Bottom) The interaction ratio w_t/χ_t at the triple point *vs* b_B/N. For w/χ above the curve, the isotropic phase is first unstable to the nematic phase, and for w/χ below the curve, the isotropic phase is first unstable to the smectic phase.

The behavior of the triple point, shown as a large dot in Figure 3a for the particular case of $b_B = 50$, is shown as a function of b_B in Figure 3b. We have plotted the ratio of anisotropic to isotropic interactions at the triple point, w_t/χ_t, as a function of b_B/N. Above the curve, the isotropic phase is first unstable to the nematic phase, and below the curve, the isotropic phase is first unstable to a microphase. According to Figure 3b, w_t/χ_t decreases as the stiffness b_B increases. This is consistent with the intuition that weaker relative anisotropic interactions should be required to drive the system into a nematic phase as the B block stiffens. It is evident from the figure that the strength of the w_t required for the system to be in the nematic phase is unphysically large unless b_B/N is nearly of order unity. For reasonable values of $w_t/\chi_t \approx 1$, the nematic phase is

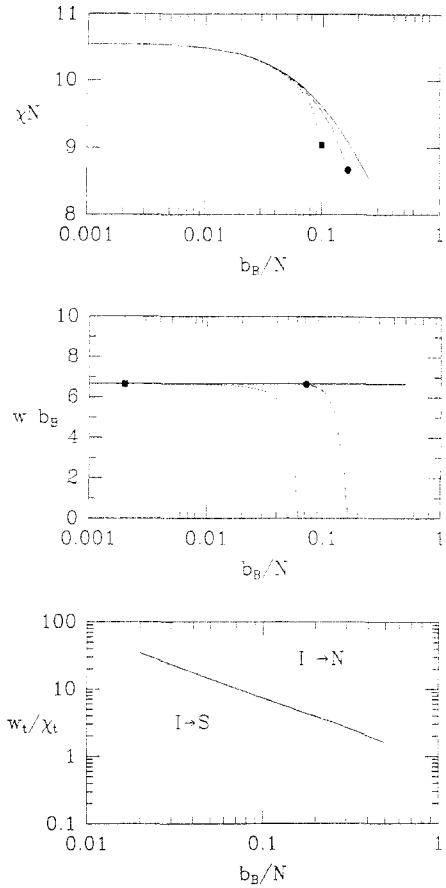

Figure 4. Phase diagrams for series II (semiflexible–semiflexible diblocks) with $N = 100$, $b_B/b_A = 2$, and $f = 0.5$. (a, Top) The spinodal value of χN *vs* b_B/N for $w = 0$ (solid), $w = 0.4$ (dashed), and $w = 0.6667$ (dotted). This figure for series II should be compared to Figure 2a for series I. The onset of the nematic phase is denoted by a large solid circle for $w = 0.4$ (dashed curve) and by a solid square for $w = 0.6667$ (dotted curve). (b, Middle) The spinodal value of wb_B *vs* b_B/N for $\chi N = 0$ (solid), $\chi N = 9.25$ (dashed), and $\chi N = 10.0$ (dotted). The curves mark the isotropic–nematic transition to the left of the solid circle ($\chi N = 9.25$) and square ($\chi N = 10.0$) and the isotropic–smectic transition to the right of the solid symbols. (c, Bottom) The interaction ratio w_t/χ_t at the triple point *vs* b_B/N. As in Figure 3b, the isotropic is first unstable to the nematic (smectic) phase for w/χ above (below) the curve.

preempted by a microphase unless the B block is nearly a rigid rod.

B. Series II: Semiflexible–Semiflexible Diblocks. In the second set of diblocks, we focus on the effect of stiffening the diblock as a whole. First we fix N and $f = 0.5$ and increase b_A and b_B in tandem, holding $b_A = b_B$. In this special case, we find that the composition and orientational order parameters decouple. This is expected, since fluctuations in composition do not affect local average stiffness and fluctuations in orientation do not affect local average composition. When the two order parameters decouple, the spinodal value of χ_s is independent of w. For flexible chains ($b_A = b_B = 1$), we find $\chi_s N = 10.5$, in agreement with Leibler. As b_A and b_B are increased, $\chi_s N$ drops monotonically, eventually reaching $\chi_s N = 8.3$ in the extreme case where each block is a rigid rod ($b_A = b_B = N/2$). We interpret the decrease of χ_s with increasing chain rigidity to be due to the decrease in the conformational entropy cost of creating the smectic phase.

The results are more dramatic when we fix the stiffness ratio of the blocks to $b_B/b_A = 2$. As before, we have also fixed N and $f = 0.5$. Thus, we begin with $b_A = 1$ and $b_B = 2$ and increase both b_A and b_B until $b_B = N/2$. In Figure 4a, we have plotted the spinodal value of $\chi_s N$ as a function of b_B/N for $w = 0$ (solid), $w = 0.4$ (dashed), and $w = 0.6667$ (dotted). Figure 4a should be compared to Figure 2a, where the same quantities have been shown for series I (flexible–semiflexible diblocks) instead of series II (semiflexible–semiflexible diblocks). The spinodal value of $\chi_s N$ decreases monotonically (the two blocks become less miscible) as b_B/N increases, but as in Figure 2a, the change in $\chi_s N$ with stiffness is numerically quite small. Again, we believe that χ_s decreases as b_B increases because the conformational entropy penalty of the smectic phase decreases as the chains stiffen. Finally, the variation of $\chi_s N$ with w is shown in the three curves of Figure 4a. As w increases, $\chi_s N$ decreases slightly, as in series I. For sufficiently large b_B at fixed $w > 0$, the microphase is preempted by the nematic phase. The onset of the nematic phase is marked by a large solid circle for $w = 0.4$ and square for $w = 0.6667$; as in Figure 2a, the onset moves to smaller b_B as w increases.

Our results in Figure 4a can be compared to the predictions of Vavasour and Whitmore,[25] who used self-consistent mean field theory to study the phase behavior of chains with $b_A \neq b_B$. Their approach is valid for $N_A \gg 1$ and $N_B \gg 1$. They find that the phase diagram should depend on the quantity $\epsilon = b_B^2/b_A^2$, in addition to χN and f, as originally predicted by Leibler. This additional dependence of the phase diagram on the ratio of the two statistical segment lengths was first suggested by Almdal and co-workers on the basis of their experimental results.[17] In Figure 4a, ϵ and f are fixed, so their results predict that $\chi_s N$ should be independent of b_B. We do indeed find that $\chi_s N$ is independent of b_B for sufficiently small b_B/N. Their prediction breaks down for $b_B/N \gtrsim 0.005$, or equivalently, for $N_B \lesssim 100$.

In Figure 4b, we have plotted the spinodal value of $w_s b_B$ as a function of b_B/N for series II with $b_B/b_A = 2$. We have fixed $\chi N = 0$ (solid), $\chi N = 9.25$ (dashed), and $\chi N = 10.0$ (dotted). Figure 4b for series II should be compared to Figure 2b for series I. In sharp contrast to Figure 2b, we see that $w_s b_B$ is independent of b_B for $\chi = 0$. When the chain is stiffened as a whole, the Maier–Saupe parameter scales inversely with b_B. This scaling is similar to the inverse scaling of χ_s with N. The latter scaling implies that the translational entropy decreases inversely with the chain length N, while the former scaling implies that the orientational entropy decreases inversely with the persistence length b_B.

The effect of increasing χ in Figure 4b is similar to Figure 2b. As χ increases, the magnitude of w required to drive the system into a nematic or microphase decreases. The triple point is marked by a large solid circle for $\chi N = 9.25$ and square for $\chi N = 10.0$. When the system is unstable to a microphase (right of the solid symbol), w decreases rapidly with large b_B and can go negative, as in series I.

The phase diagram for fixed b_A and b_B is qualitatively the same as Figure 3a, so it is not shown here. In Figure 4c, we plot the triple point interaction ratio w_t/χ_t *vs* b_B/N. In this case, the behavior is particularly simple: w_t/χ_t scales inversely with b_B, so it appears as a straight line on a log–log plot. As in Figure 3b, however, it is clear that for physical values of w_t/χ_t, the nematic phase will be precluded by a microphase unless the two blocks are nearly rigid. This is consistent with the conclusions of a recent fluctuation analysis of symmetric flexible diblocks by Morse and Milner.[43]

C. Series III: Rod–Semiflexible Diblocks. In the third series of diblocks, we hold the A block fixed as a single rod: $b_A = N/2$. Again, we hold $f = 0.5$ and N fixed. We vary the B block from a flexible coil to a rod, so the diblock varies from a rodcoil copolymer to two rods

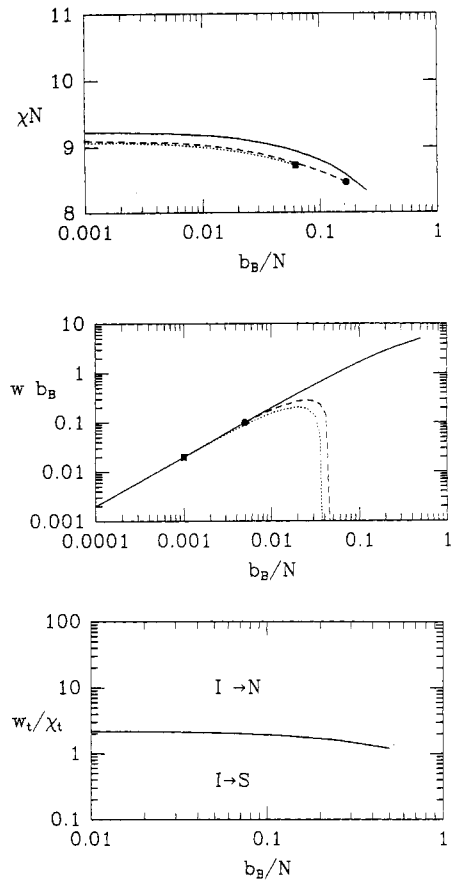

Figure 5. Phase diagrams for series III (rod–semiflexible diblocks) with $N = 20000$, $b_A = 10000$, and $N_A = 1$. The B block varies from $b_B = 1$ to $b_B = 10000$ with $N_B = 10000/b_B$. (a, Top) The spinodal value of χN *vs* b_B/N for $w = 0$ (solid), $w = 8.0 \times 10^{-4}$ (dashed), and $w = 8.8 \times 10^{-4}$ (dotted). As in Figures 2a and 4a, the triple point is marked by a large circle for the dashed curve and square for the dotted curve. (b, Middle) The spinodal value of wb_B *vs* b_B/N for $\chi N = 0$ (solid), $\chi N = 9.0$ (dashed), and $\chi N = 9.04$ (dotted). The triple point is marked by a large solid circle (square) for the dashed (dotted) curve. (c, Bottom) The ratio w_t/χ_t at the triple point *vs* b_B/N. This should be compared to Figures 3b and 4c for series I and II.

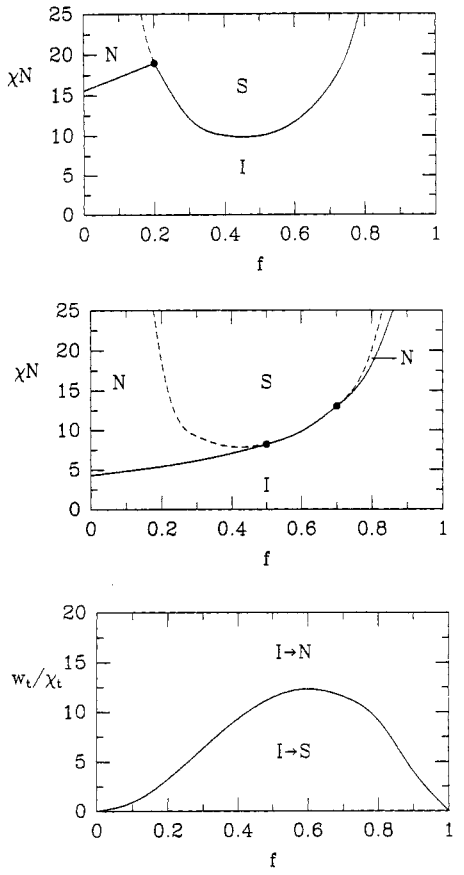

Figure 6. Composition phase diagrams for series IV (flexible–semiflexible diblocks) with $N = 200$, $b_A = 1$, and $b_B = 20$. The volume fraction f is varied by changing N_A and N_B. (a, Top) χN *vs* f for fixed $w/\chi = 3.2$. The triple point is denoted by a large dot. Transitions from the isotropic phase are shown as solid lines; the smectic spinodal preempted by the nematic phase is depicted as a dashed line. (b, Middle) χN *vs* f for fixed $w/\chi = 11.4$. The triple points are marked by large dots. Note that the nematic phase appears at large f also. This is because the ratio w/χ is fixed and the spinodal χ diverges when f approaches unity; see text. (c, Bottom) Triple point ratio w_t/χ_t *vs* f. For w/χ above (below) the curve, the isotropic phase is first unstable to the nematic (smectic) phase. Note that for sufficiently large w/χ, the isotropic phase is first unstable to the nematic phase for all f.

connected by a free joint.

Figure 5a shows the spinodal value of $\chi_s N$ as a function of b_B/N and should be compared to Figure 2a and 4a. In this case, we have fixed $w = 0$ (solid), $w = 8.0 \times 10^{-4}$ (dashed), and $w = 8.8 \times 10^{-4}$ (dotted). As before, $\chi_s N$ decreases as b_B increases. The trend with increasing w is rather different, however. In Figures 2a and 4a, increasing w has little effect until b_B/N is fairly large. In Figure 5a, on the other hand, w has a significant effect at small b_B. We believe this is because w has more effect when the *difference* in stiffness is larger. The nematic fluctuations that enhance phase separation are stronger when the difference in stiffness is larger. As in Figures 2a and 4a, the onset of the nematic phase (denoted by a large solid circle for $w = 8.0 \times 10^{-4}$ and square for $w = 8.8 \times 10^{-4}$) moves to lower b_B as w increases. In the extreme limit where b_B is small, our results agree with those of Holyst and Schick.[33]

In Figure 5b, we display the spinodal value of $w_s b_B$ *vs* b_B/N for $\chi N = 0$ (solid), $\chi N = 9.0$ (dashed), and $\chi N = 9.04$ (dotted). In this case, where there is a large difference in stiffness in the two blocks, $w_s b_B$ is not constant. This is similar to Figure 2b and should be contrasted with Figure 4b. Again, the onset of the microphase is marked by large solid circle for $\chi N = 9.0$ and square for $\chi N = 9.04$.

Finally, in Figure 5c, we show the behavior of the triple point ratio w_t/χ_t as a function of b_B/N. In this series, where the A block is always a rigid rod, the ratio $w_t/\chi t$ remains nearly constant until the B block is also fairly rigid. Moreover, the magnitude of w_t/χ_t lies in the physical range for all b_B. This implies that the A block is primarily responsible for nematic order, until the B block becomes rigid enough to contribute.

D. Series IV: Composition Dependence of Flexible–Semiflexible Diblocks. In the last two series of diblocks, series IV and V, we explore the phase behavior as a function of volume fraction f. In series IV, we hold $b_A = 1$, $b_B = 20$, and $N = 200$ fixed and vary $f = N_A b_A/N$ by adjusting N_A and N_B. The resulting phase diagrams of χN *vs* f are shown in Figures 6a and 6b for $w/\chi = 3.2$ and $w/\chi = 11.4$, respectively. These phase diagrams should be compared to Figure 8 of Leibler's paper[19] for symmetric flexible diblocks and to Figure 1 of Holyst and Schick's paper[33] for rodcoil diblocks. Our system lies somewhere between these two extremes, but its phase diagrams are qualitatively identical to those of rodcoil diblocks.[33] The solid lines in Figures 6a and 6b denote phase boundaries between the isotropic phase and a microphase or nematic phase. The dashed lines represent the instability of the

isotropic phase to microphase separation, preempted by the isotropic–nematic boundary. The true nematic–microphase boundary may lie near the dashed lines. The triple point is marked by a large dot. Note that our approximation of the spinodal as the phase boundary breaks down for f far from $f = 0.5$. In the case $b_A = b_B \ll N$ studied by Leibler,[19] the spinodal is a fairly close approximation to the actual phase boundary between the microphases and the isotropic phase, but the discrepancy between the spinodal and the phase boundary may be greater when $b_A \neq b_B$.

According to Figure 6b, the nematic phase preempts the microphase at large f as well as small f. This is surprising, since one would expect it to be harder to form a nematic phase when the volume fraction of the flexible component is high. In a phase diagram as a function of *temperature* rather than χ, we believe that the nematic phase at high f would not be present. It occurs in Figure 6b because we have fixed the ratio w/χ. Although the interaction strength w_s required to drive the system into the nematic phase increases with f, the strength of χ_s needed to obtain a microphase also increases as f approaches unity. From Leibler's calculations, we find that the microphase spinodal χ_s diverges as $1/(1-f)^2$ near $f = 1$. We expect the nematic spinodal w_s, on the other hand, to obey[4] $w_s \sim 1/(fb_A + (1-f)b_B)$. For fixed w/χ, therefore, we find that the microphase requires such a large χ_s for large f that it is preempted by the nematic phase.

We now turn to a detailed examination of Figures 6a and 6b. In the flexible case studied by Leibler, the minimum of the isotropic–microphase boundary occurs at $f = 0.5$, due to his assumed equality of statistical segment lengths. In the asymmetric case of series IV or rodcoil diblocks, however, the minimum is shifted to $f < 0.5$, toward a higher volume fraction of the stiffer component B. This is consistent with the notion of spontaneous curvature in the microphase. As discussed for Figure 2a for $f = 0.5$, there is a spontaneous curvature favoring the stiffer component on the inside, because the elastic cost of stretching chains is lower for stiffer chains. As the volume fraction of the stiff component increases, or f decreases, this counteracts the stiffness ratio, decreasing the spontaneous curvature. The shift in the phase boundary follows the vanishing of the spontaneous curvature. This trend is consistent with calculations of Milner[41] in the WSL as well as trends in the lamellar–cylinder and cylinder–sphere transitions predicted by Ouimet and Fredrickson[42] in the SSL.

By comparing Figures 6a and 6b, we observe that the system becomes less miscible as w is increased. A smaller χ is required for microphase separation to occur. As in Figures 2a, 4a, and 5a, we attribute this to nematic fluctuations that orient the stiffer component and expel the more flexible component. In addition, we see growth of the nematic phase with w. For smaller w (Figure 6a), the nematic phase precludes the microphase only for large volume fractions of the stiffer component (small f). As the anisotropic interaction strength increases, however (Figure 6b), the nematic phase preempts microphase separation over a larger range of f. The triple point shifts to lower χN and larger f, as expected.

Finally, Figure 6c shows the triple point ratio w_t/χ_t as a function of f for series IV. For $f \lesssim 0.6$, w_t/χ_t increases. This is expected, because the strength of w needed to obtain a nematic phase should increase as the volume fraction of the flexible component increases. For $f \gtrsim 0.6$, however, the ratio decreases. This is consistent with Figure 6a, where we see that the nematic phase preempts the microphase for large f. As discussed for Figure 6a, the ratio w_t/χ_t decreases because χ_t diverges in the limit $f \to 1$ while w_t approaches a constant value.

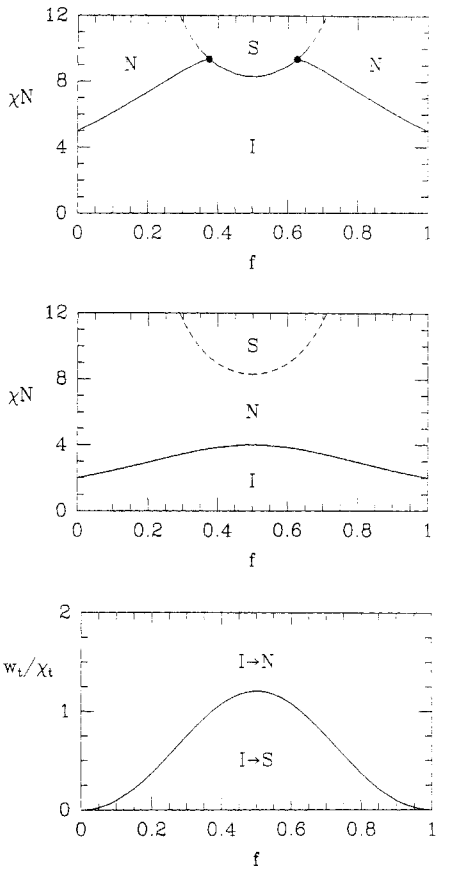

Figure 7. Composition phase diagrams for series V (rod–rod diblocks) with $N = 1000$, $N_A = 1$, and $N_B = 1$. The volume fraction f is adjusted by varying b_A and b_B. (a, Top) χN *vs* f for fixed $w/\chi = 1.0$. As in Figure 6, the triple points are marked by large dots and preempted spinodals are shown as dashed lines. (b, Middle) χN *vs* f for fixed $w/\chi = 2.5$. At this ratio, the isotropic phase is first unstable to the nematic phase at all f, so there is no triple point. (c, Bottom) Triple point ratio w_t/χ_t *vs* f. As in Figure 6c, the system is first unstable to the smectic phase only for small w/χ and f not too close to zero or one; see text.

E. Series V: Composition Dependence of Rod–Rod Diblocks. In this last series of diblocks, we fix N, $N_A = 1$ and $N_B = 1$. Thus, the diblock always consists of two rods, one of species A and one of species B. The volume fraction f is varied by changing the rod lengths b_A and b_B. The phase diagrams shown in Figures 7a and 7b are symmetric around $f = 0.5$, due to symmetry in stiffness. We have fixed the interaction strength ratio w/χ to be $w/\chi = 1.0$ and $w/\chi = 2.5$ in Figures 7a and 7b, respectively.

In Figure 7a, the minimum of the isotropic–microphase boundary occurs at $\chi_s N = 8.3$, which is significantly lower than the Leibler value of $\chi N = 10.5$. For this physically reasonable value of $w/\chi = 1.0$, large regions of the phase diagram are nematic, because the two blocks are rigid. The isotropic–nematic boundary moves to lower $\chi_s N$ as the volume fraction is varied away from $f = 0.5$. The value of w required to drive the system into a nematic phase is roughly $w_s \sim 1/b$, which is twice as large at $f = 0.5$ as at $f = 0$ and $f = 1$. Since the ratio w/χ is fixed, the spinodal value of χ_s is also twice as large at $f = 0.5$ as at $f = 0$ and $f = 1$. For the stronger, but still physical, ratio of $w/\chi = 2.5$, the phase diagram in Figure 7b is quite different. Microphase separation is now always precluded by the nematic phase. The microphase spinodal is the dashed curve. Note that the isotropic–nematic phase boundary

bows upward toward the microphase spinodal, as in Figure 7a. The spinodal value at $f = 0.5$ ($\chi N = 4.0$) is again twice as large as the value at $f = 0$ and $f = 1$ ($\chi N = 2.0$).

In Figure 7c, we have plotted the triple point ratio w_t/χ_t as a function of composition. This ratio vanishes at $f = 0$ and $f = 1$ because the value of χ_t needed to obtain a microphase diverges in those limits, as discussed in subsection D. In addition, the value of $w_t \sim 1/(fb_A + (1-f)b_B) = 1/N(f^2 + (1-f)^2)$ required to achieve a nematic phase also decreases as f moves away from $f = 0.5$. This is because the strength of the anisotropic interaction at the spinodal is dominated by the length of the longer rod, which increases as f moves away from $f = 0.5$. Note that no triple point exists beyond roughly $w_t/\chi_t = 1.2$, in agreement with Figure 7b.

Finally, we note that the isotropic–nematic transition should be relatively insensitive to the connectivity between the two blocks. Thus, the isotropic–nematic transition should be roughly the same for rod–rod diblocks as for rod–rod mixtures. Rod–rod mixtures have been studied by Holyst and Schick,[34] and, indeed, Figure 7b is very similar to their Figure 5.

V. Discussion

The coupling between the composition and orientational order parameters gives rise to strong fluctuation effects in diblock copolymers when there is a difference in the stiffnesses of the two blocks. For example, nematic fluctuations enhanced by a large anisotropic interaction, tend to align stiff segments. Since flexible blocks lose conformational entropy when they align, the flexible component prefers to demix from the oriented stiff-rich regions, promoting the early onset of microphase separation. A similar mechanism has been demonstrated in semiflexible homopolymer blends.[2,3] Conversely, microphase fluctuations enhanced by a large isotropic interaction tend to concentrate stiff segments. These segments then each feel an enhanced nematic potential, leading to early onset of the nematic phase. These fluctuation effects are stronger when the stiffness difference is large.

There are other ways in which chain stiffness affects phase behavior in diblocks. For example, differences in stiffnesses can give rise to spontaneous curvature in the smectic phase. In addition, there is a conformational entropy cost in forming the smectic phase, since chains tend to be stretched in the direction of translational order. There is a smaller entropy cost for stretching stiff chains then flexible ones, so the smectic phase is more favorable for stiff chains. By the same token, it costs less entropy to align stiff chains than flexible ones, so the smectic phase is more favorable for stiff chains. If the blocks are sufficiently stiff, and anisotropic interactions sufficiently strong, then the isotropic–nematic transition can preclude the isotropic–smectic transition.

In this study, we carried the Landau–Ginzburg expansion of the free energy to quadratic order only. Given the difficulty of carrying out the Legendre transformation at this order (see Appendix B), it seems prohibitively time-consuming to extend the expansion to higher order. Unfortunately, our second-order analysis is not sufficient to distinguish the smectic phase from the wide variety of ordered micellar phases predicted for semiflexible diblocks. Moreover, our analysis cannot extend into the low-temperature region, where the smectic C and bilayer lamellae phases are predicted to exist. Nonetheless, the weak segregation analysis presented here reveals interesting trends with stiffness and stiffness difference that should aid experimental work in the rich area of semiflexible copolymer thermodynamics.

Acknowledgment. We are grateful to M. Schick and R. Holyst for helping us find an error in our calculations and to J. P. Donley and S. T. Milner for instructive discussions. This work was supported by the MRL Program of the National Science Foundation under Grant No. DMR-9123048 (A.J.L.), by NSF-DMR-8906783 (C.S.), by NSF-PHYS-9116964 (M.G.), and by the Camille and Henry Dreyfus Foundation.

Appendix A: Calculation of Correlation Functions

Here we provide a brief sketch of the calculation of various noninteracting pair correlation functions needed for the free energy functional. We shall only show the derivation of $G^{ij}_{\phi_A S_A}(\mathbf{k}) \equiv \langle \phi_A(\mathbf{k})\, S^{ij}_A(-\mathbf{k})\rangle$ for a single chain of freely jointed rigid rods, but other correlation functions can be computed in an analogous way.

The correlation function $G^{ij}_{\phi_A S_A}(\mathbf{k})$ is the Fourier transform of the correlation function $G^{ij}_{\phi_A S_A}(\vec{r} - \vec{r}') \equiv \langle \phi_A(\vec{r})\, S^{ij}_A(\vec{r}')\rangle$. In terms of the microscopic variables, the correlation function can be written as

$$G^{ij}_{\phi_A S_A}(\mathbf{k}) = \sum_{\substack{\{n=1\}\\ \{n'=1\}}}^{N_A} \int_{-b_A/2}^{b_A/2} ds\, ds' \langle Q^{ij}(\vec{u}_n') \exp[-i\mathbf{k}\cdot((\vec{r}_n + a_0 s\vec{u}_n) - (\vec{r}_n' + a_0 s'\vec{u}_n'))]\rangle \quad \text{(A1)}$$

where

$$Q^{ij}(\vec{u}_n') = \left[u_n^{i\prime} u_n^{j\prime} - \frac{1}{3}\delta^{ij}\right] \quad \text{(A2)}$$

The angular brackets in eq A1 denote thermodynamic averages. In our case of freely jointed rods, the thermodynamic average is taken by integrating over all possible orientations of the rods on the chain.

We now separate the sums over n and n' into a rod contribution, where $n = n'$, describing correlations within a single rod, and a flexible contribution, describing correlations between different rods on the same chain:

$$G^{ij}_{\phi_A S_A}(\mathbf{k}) = \sum_{n=1}^{N_A} G^{ij}_{\text{rod}} + \sum_{n' \neq n}^{N_A} G^{ij}_{\text{flex}} \quad \text{(A3)}$$

where

$$G^{ij}_{\text{rod}} = \int_{-b_A/2}^{b_A/2} ds\, ds' \langle Q^{ij}(\vec{u}_n) \exp[-i\mathbf{k}a_0\cdot(s-s')\vec{u}_n]\rangle \quad \text{(A4)}$$

and

$$G^{ij}_{\text{flex}} = \int_{-b_A/2}^{b_A/2} ds\, ds' \langle Q^{ij}(\vec{u}_n') \exp[-i\mathbf{k}\cdot(\vec{r}_n - \vec{r}_n')] \times \exp[-i\mathbf{k}a_0\cdot(s\vec{u}_n - s'\vec{u}_n')]\rangle \quad \text{(A5)}$$

Note that Q^{ij} is a linear combination of spherical harmonics Y_{lm} of order $l = 2$. We expand the exponential in eq A4 in spherical harmonics and use orthogonality of spherical harmonics to obtain

$$G^{ij}_{\text{rod}} = -\Delta^{ij}(\hat{k})\, \beta_r(q, b_A) \quad \text{(A6)}$$

where $q = ka_0$ is dimensionless and

$$\beta_r(q, b_A) = \frac{1}{q^2}[3j_0(qb_A) + \cos(qb_A) + qb_A\, \text{Si}(qb_A) - 4] \quad \text{(A7)}$$

and

$$\Delta^{ij}(\hat{k}) = \hat{k}_i\hat{k}_j - \frac{1}{3}\delta^{ij} \tag{A8}$$

In eq A7, $j_0(x)$ is the zeroth-order spherical Bessel function and $Si(x)$ is the sine integral function.[44]

To calculate G^{ij}_{flex}, we note that

$$\vec{r}_n - \vec{r}_{n'} = b_A\left[\frac{1}{2}(\vec{u}_n + \vec{u}_{n'}) + \sum_{m=n'+1}^{n-1}\vec{u}_m\right] \tag{A9}$$

Moreover, since the rods are freely jointed, the integrals over all possible orientations in the thermodynamic average are independent for different rods. Thus, the ensemble average of products over various rods can be replaced by the product of angular averages.

$$G^{ij}_{flex} = \int_{-b_A/2}^{b_A/2}ds\,ds' \times \prod_{m=n'+1}^{n-1}\langle\exp[-i\mathbf{k}a_0\cdot\vec{u}_m b_A]\rangle\langle\exp[-i\mathbf{k}a_0\cdot\vec{u}_n(b_A/2+s)]\rangle \times \langle Q^{ij}(\vec{u}_{n'})\exp[-i\mathbf{k}a_0\cdot\vec{u}_{n'}(b_A/2-s')]\rangle \tag{A10}$$

Again, we expand the exponentials in spherical harmonics and carry out the angular integrals. Our result is

$$G^{ij}_{flex} = -\Delta^{ij}(\hat{k})(j_0(qb_A))^{n-n'-1}\beta_f(q,b_A)\,\alpha_f(q,b_A) \tag{A11}$$

where

$$\alpha_f(q,b_A) = Si(qb_A)/q$$

$$\beta_f(q,b_A) = \frac{1}{2q}[Si(qb_A) - 3j_1(qb_A)] \tag{A12}$$

Finally, we substitute eqs A6 and A11 into eq A3 to obtain the final result:

$$G^{ij}_{\phi_A S_A}(\mathbf{k}) = -\Delta^{ij}(\hat{k})[N_A\beta_r(q,b_A) + h(N_A,j_0(qb_A))\alpha_f(q,b_A)\,\beta_f(q,b_A)] \tag{A13}$$

where

$$h(N,y) = \sum_{n'\neq n}^{N} y^{n-n'-1} = 2\left[\frac{N-1}{1-y} - \frac{y(1-y^{N-1})}{(1-y)^2}\right] \tag{A14}$$

The procedure for deriving other pair correlation functions is a straightforward extension of the calculation above. Here we only cite some of the results. We find

$$G_{\phi A\phi A}(\mathbf{k}) \equiv \langle\phi_A(k)\,\phi_A(-k)\rangle = N_A\alpha_r(q,b_A) + h(N_A,j_0(qb_A))\alpha_f^2(q,b_A) \tag{A15}$$

where

$$\alpha_r(q,b_A) = \frac{2b_A\,Si(qb_A)}{q} - b_A{}^2[j_0(qb_A/2)]^2 \tag{A16}$$

Also,

$$G^{ijkl}_{S_A S_A}(\mathbf{k}) \equiv \langle S^{ij}_A(\mathbf{k})\,S^{kl}_A(-\mathbf{k})\rangle \equiv \sum_{n=1}^{4}[N_A\gamma_r^{(n)}(q,b_A) + h(N_A,j_0(qb_A))\beta_f^2(q,b_A)\,\gamma_f^{(n)}(q,b_A)]D_n^{ijkl}(\hat{k}) \tag{A17}$$

where $D_n^{ijkl}(\hat{k})$ are four fourth-rank tensors given by

$$D_1^{ijkl}(\hat{k}) = \frac{1}{2}(\delta^{ik}\delta^{jl} + \delta^{il}\delta^{jk})$$

$$D_2^{ijkl}(\hat{k}) = \frac{1}{3}\delta^{ij}\delta^{kl}$$

$$D_3^{ijkl}(\hat{k}) = \frac{1}{4}(\hat{k}_i\hat{k}_k\delta^{jl} + \hat{k}_j\hat{k}_l\delta^{ik} + \hat{k}_i\hat{k}_l\delta^{jk} + \hat{k}_j\hat{k}_k\delta^{il}) - \frac{1}{3}(\hat{k}_i\hat{k}_j\delta^{kl} + \hat{k}_k\hat{k}_l\delta^{ij})$$

$$D_4^{ijkl}(\hat{k}) = \hat{k}_i\hat{k}_j\hat{k}_k\hat{k}_l - \frac{1}{3}(\hat{k}_i\hat{k}_j\delta^{kl} + \hat{k}_k\hat{k}_l\delta^{ij}) \tag{A18}$$

The coefficients $\gamma_r^{(n)}$ and $\gamma_f^{(n)}$ are

$$\gamma_r^{(1)} = \frac{1}{6q^2}[-8 + 5j_0(qb_A) + 2j_2(qb_A) + 3\cos(qb_A) + 3qb_A\,Si(qb_A)]$$

$$\gamma_r^{(2)} = \frac{1}{12q^2}[16 - 9j_0(qb_A) + 6j_2(qb_A) - 7\cos(qb_A) - 7qb_A\,Si(qb_A)]$$

$$\gamma_r^{(3)} = \frac{1}{3q^2}[16 - 13j_0(qb_A) - 10j_2(qb_A) - 3\cos(qb_A) - 3qb_A\,Si\,k]$$

$$\gamma_r^{(4)} = 3\gamma_r^{(1)} + 3\gamma_r^{(2)} - \gamma_r^{(3)} \tag{A19}$$

and

$$\gamma_f^{(1)} = 0$$

$$\gamma_f^{(2)} = 1/3$$

$$\gamma_f^{(3)} = 0$$

$$\gamma_f^{(4)} = 3\gamma_f^{(1)} + 3\gamma_f^{(2)} - \gamma_f^{(3)} = 1 \tag{A20}$$

Note that only three of the four coefficients of $D_n^{ijkl}(\hat{k})$ are independent since the orientational density describes uniaxial nematic order.

Appendix B: Legendre Transformation

The entropic part of the free energy, within the random phase approximation, can be extracted from the noninteracting correlation functions by performing a Legendre transformation. We first introduce conjugate fields to the order parameters. We define $h_{\phi_A}(\mathbf{k})$, $h_{\phi_B}(\mathbf{k})$, $\vec{h}_{S_A(\mathbf{k})}$, and $\vec{h}_{S_B(\mathbf{k})}$ conjugate to $\phi_A(\mathbf{k})$, $\phi_B(\mathbf{k})$, $\vec{S}_A$, and $\vec{S}_B$, respectively. Next, the thermodynamic potential $\mathcal{W}$ is expanded to quadratic order in the conjugate fields. A more detailed discussion of this step is provided in section III of Leibler's paper.[19] For convenience, we now cast the order param-

eters and conjugate fields in matrix form:

$$\Phi(\mathbf{k}) = \begin{pmatrix} \phi_A(\mathbf{k}) \\ \phi_B(\mathbf{k}) \end{pmatrix}$$

$$\mathcal{S}^{ij}(\mathbf{k}) = \begin{pmatrix} S_A^{ij} \\ S_B^{ij} \end{pmatrix} \tag{B1}$$

and

$$\mathbf{h}_\phi(\mathbf{k}) = \begin{pmatrix} h_{\phi_A}(\mathbf{k}) \\ h_{\phi_B}(\mathbf{k}) \end{pmatrix} \tag{B2}$$

$$\mathbf{h}_S^{ij}(\mathbf{k}) = \begin{pmatrix} h_{S_A}^{ij}(\mathbf{k}) \\ h_{S_A}^{ij}(\mathbf{k}) \end{pmatrix} \tag{B3}$$

Similarly, we write the correlation functions as 2 × 2 matrices:

$$\mathcal{G}_{\phi\phi}(\mathbf{k}) = \begin{pmatrix} G_{\phi_A\phi_A}(\mathbf{k}) & G_{\phi_A\phi_B}(\mathbf{k}) \\ G_{\phi_A\phi_B}(\mathbf{k}) & G_{\phi_B\phi_B}(\mathbf{k}) \end{pmatrix} \tag{B4}$$

$$\mathcal{G}_{\phi S}^{ij}(\mathbf{k}) = \begin{pmatrix} G_{\phi_A S_A}^{ij}(\mathbf{k}) & G_{\phi_A S_B}^{ij}(\mathbf{k}) \\ G_{\phi_B S_A}^{ij}(\mathbf{k}) & G_{\phi_B S_B}^{ij}(\mathbf{k}) \end{pmatrix} \tag{B5}$$

$$\mathcal{G}_{SS}^{ijkl}(\mathbf{k}) = \begin{pmatrix} G_{S_A S_A}^{ijkl}(\mathbf{k}) & G_{S_A S_B}^{ijkl}(\mathbf{k}) \\ G_{S_A S_B}^{ijkl}(\mathbf{k}) & G_{S_B S_B}^{ijkl}(\mathbf{k}) \end{pmatrix} \tag{B6}$$

We now construct larger vectors and matrices:

$$\Phi^{ij}(\mathbf{k}) = \begin{pmatrix} \Phi(\mathbf{k}) \\ \mathcal{S}^{ij}(\mathbf{k}) \end{pmatrix}$$

$$\mathbf{h}^{ij}(\mathbf{k}) = \begin{pmatrix} \mathbf{h}_\phi(\mathbf{k}) \\ \mathbf{h}_S^{ij}(\mathbf{k}) \end{pmatrix} \tag{B7}$$

and

$$\mathcal{G}^{ijkl}(\mathbf{k}) = \begin{pmatrix} \mathcal{G}_{\phi\phi}(\mathbf{k}) & \mathcal{G}_{\phi S}^{ij}(\mathbf{k}) \\ \mathcal{G}_{\phi S}^{kl}(\mathbf{k})^T & \mathcal{G}_{SS}^{ijkl}(\mathbf{k}) \end{pmatrix} \tag{B8}$$

The entropic part of the thermodynamic potential can then be written compactly as

$$\mathcal{W} = \frac{1}{2}\sum_{\mathbf{k}} \mathbf{h}^{ij}(\mathbf{k})^\dagger \cdot \mathcal{G}^{ijkl}(\mathbf{k}) \cdot \mathbf{h}^{kl}(\mathbf{k}) \tag{B9}$$

Note that $\mathcal{W}$ should actually be written as an expansion in powers of the conjugate fields; here, we have truncated the expansion at quadratic order. In eq B9 and all subsequent equations, summation over repeated indices is implied.

Our aim is to find the entropic part of the Helmholtz free energy $\mathcal{F}$ in terms of the order parameters:

$$\mathcal{F} = \sum_{\mathbf{k}} \mathbf{h}^{ij}(\mathbf{k})^\dagger \cdot \Psi^{ij}(\mathbf{k}) - \mathcal{W} \tag{B10}$$

We must first solve for the order parameters in terms of the fields by using the equation of state:

$$\Psi^{ij}(\mathbf{k}) = \frac{\delta \mathcal{W}}{\delta \mathbf{h}^{ij}(\mathbf{k})^\dagger} \tag{B11}$$

We now assume that the Helmholtz free energy has the form

$$\mathcal{F} = \frac{1}{2}\sum_{\mathbf{k}} \Psi^{ij}(\mathbf{k})^\dagger \cdot \mathcal{H}^{ijkl}(\mathbf{k}) \cdot \Psi^{kl}(\mathbf{k}) \tag{B12}$$

where $\mathcal{H}(\mathbf{k})$ has the same form as $\mathcal{G}(\mathbf{k})$:

$$\mathcal{H}^{ijkl}(\mathbf{k}) = \begin{bmatrix} \mathcal{H}_{\phi_A\phi_A}(\mathbf{k}) & \mathcal{H}_{\phi_A\phi_B}(\mathbf{k}) & \mathcal{H}_{\phi_A S_A}^{ij}(\mathbf{k}) & \mathcal{H}_{\phi_A S_B}^{ij}(\mathbf{k}) \\ \mathcal{H}_{\phi_A\phi_B}(\mathbf{k}) & \mathcal{H}_{\phi_B\phi_B}(\mathbf{k}) & \mathcal{H}_{\phi_B S_A}^{ij}(\mathbf{k}) & \mathcal{H}_{\phi_B S_B}^{ij}(\mathbf{k}) \\ \mathcal{H}_{\phi_A S_A}^{kl}(\mathbf{k}) & \mathcal{H}_{\phi_B S_A}^{kl}(\mathbf{k}) & \mathcal{H}_{S_A S_A}^{ijkl}(\mathbf{k}) & \mathcal{H}_{S_A S_B}^{ijkl}(\mathbf{k}) \\ \mathcal{H}_{\phi_A S_B}^{kl}(\mathbf{k}) & \mathcal{H}_{\phi_B S_B}^{kl}(\mathbf{k}) & \mathcal{H}_{S_A S_B}^{ijkl}(\mathbf{k}) & \mathcal{H}_{S_B S_B}^{ijkl}(\mathbf{k}) \end{bmatrix} \tag{B13}$$

and solve for $\mathcal{H}(\mathbf{k})$ in terms of $\mathcal{G}(\mathbf{k})$ by inverting eq B11 and substituting into eq B9 to obtain

$$\mathcal{G}^{klmn}(\mathbf{k}) \cdot \mathcal{H}^{ijkl}(\mathbf{k}) \cdot \mathcal{G}^{opij}(\mathbf{k}) = \mathcal{G}^{opmn}(\mathbf{k}) \tag{B14}$$

Recall that the correlation functions have the form

$$\mathcal{G}_{\phi S}^{ij}(\mathbf{k}) = g_{\phi S}(\mathbf{k})\, \Delta^{ij}(\hat{k})$$

$$\mathcal{G}_{SS}^{ijkl}(\mathbf{k}) = g_{SS}^{(n)}(\mathbf{k})\, D_n^{ijkl}(\hat{k}) \tag{B15}$$

We further assume that the vertex functions $\mathcal{H}(\mathbf{k})$ have the same form:

$$\mathcal{H}_{\phi S}^{ij}(\mathbf{k}) = H_{\phi S}(\mathbf{k})\, \Delta^{ij}(\hat{k})$$

$$\mathcal{H}_{SS}^{ijkl}(\mathbf{k}) = H_{SS}^{(n)}(\mathbf{k})\, D_n^{ijkl}(\hat{k}) \tag{B16}$$

where $g_{\phi S}(\mathbf{k})$, $g_{SS}^{(n)}(\mathbf{k})$, $h_{\phi S}(\mathbf{k})$, and $h_{SS}^{(n)}(\mathbf{k})$ are all 2 × 2 matrices.

We now introduce a new matrix $\mathcal{T}(\mathbf{k})$:

$$\mathcal{T}^{ijkl}(\mathbf{k}) = \begin{bmatrix} 1 & 0 & 0 & 0 \\ 0 & 1 & 0 & 0 \\ 0 & 0 & D_1^{ijkl}(\hat{k}) & 0 \\ 0 & 0 & 0 & D_1^{ijkl}(\hat{k}) \end{bmatrix} \tag{B17}$$

and observe that

$$\mathcal{T}^{ijmn}(\mathbf{k}) \cdot \mathcal{G}^{opij}(\mathbf{k}) = \mathcal{G}^{opmn}(\mathbf{k}) \tag{B18}$$

We now substitute eq B18 into eq B14 to obtain

$$\mathcal{G}^{klmn}(\mathbf{k}) \cdot \mathcal{H}^{ijkl}(\mathbf{k}) = \mathcal{T}^{ijmn}(\mathbf{k}) \tag{B19}$$

This yields a set of equations for $H_{\phi\phi}(\mathbf{k})$, $H_{\phi S}(\mathbf{k})$, and $H_{SS}^{(n)}(\mathbf{k})$ that we can solve.

In terms of the scalar orientational order parameters defined in eq 2.6, the free energy in eq B10 can then be written as

$$\mathcal{F} = \sum_{\mathbf{k}} \frac{1}{2}\Phi(\mathbf{k})^\dagger [H_{\phi\phi}(\mathbf{k}) - \chi]\Phi(\mathbf{k}) + \frac{1}{3}[\Phi(\mathbf{k})^\dagger H_{\phi S}(\mathbf{k})\mathcal{S}(\mathbf{k}) + \mathcal{S}(\mathbf{k})^\dagger H_{\phi S}(\mathbf{k})^T \Phi(\mathbf{k})] + \frac{1}{3}\mathcal{S}(\mathbf{k})^\dagger [\tilde{H}_{SS}(\mathbf{k}) - \mathbf{w}]\mathcal{S}(\mathbf{k}) \tag{B20}$$

where the interaction matrices are

$$\chi = \begin{pmatrix} \chi_{AA} & \chi_{AB} \\ \chi_{AB} & \chi_{BB} \end{pmatrix} \tag{B21}$$

and

$$\mathbf{w} = \begin{pmatrix} w_A & w_{AB} \\ w_{AB} & w_B \end{pmatrix} \tag{B22}$$

In eq B20, we have introduced $\tilde{H}_{SS}(\mathbf{k})$, which is a linear

combination of the $H_{SS}^{(n)}(\mathbf{k})$ matrices. In the case where both directors $\hat{n}_A$ and $\hat{n}_B$ are parallel to $\mathbf{k}$ (smectic A phase), we find $\tilde{H}_{SS}(\mathbf{k}) = H_{SS}^{(1)}(\mathbf{k}) + (2/3)H_{SS}^{(3)}(\mathbf{k}) + (2/3)H_{SS}^{(4)}(\mathbf{k})$. The interested reader is encouraged to contact us for the more general case.

The final results are

$$H_{\phi\phi}(\mathbf{k}) = g_{\phi\phi}(\mathbf{k})^{-1} + \frac{2}{3}g_{\phi\phi}(\mathbf{k})^{-1}\, g_{\phi s}(\mathbf{k})\, x(\mathbf{k})^{\mathrm{T}}\, g_{\phi\phi}(\mathbf{k})^{-1} \tag{B23}$$

$$H_{\phi S}(\mathbf{k}) = -g_{\phi\phi}(\mathbf{k})^{-1}\, x(\mathbf{k}) \tag{B24}$$

and

$$\tilde{H}_{SS}(\mathbf{k}) = g_{\phi S}(\mathbf{k})^{-1}\, x(\mathbf{k}) \tag{B25}$$

where

$$x(\mathbf{k}) = \left[\left(g_{SS}^{(1)}(\mathbf{k}) + \frac{2}{3}g_{SS}^{(3)}(\mathbf{k}) + \frac{2}{3}g_{SS}^{(4)}(\mathbf{k})\right)g_{\phi S}(\mathbf{k})^{-1} - \frac{2}{3}g_{\phi S}(\mathbf{k})^{\mathrm{T}}\, g_{\phi\phi}(\mathbf{k})^{-1}\right]^{-1} \tag{B26}$$

Finally, we note that eq B20 can be written in the form of eq 2.7 by applying the incompressibility condition[36]

$$\phi_A(\mathbf{k}) = -\phi_B(\mathbf{k}) \tag{B27}$$

The coefficients $A(\mathbf{k})$, $B_A(\mathbf{k})$, etc. in eq 2.7 are given explicitly by

$$A(\mathbf{k}) = [H_{\phi\phi}(\mathbf{k})]_{11} + [H_{\phi\phi}(\mathbf{k})]_{22} + [H_{\phi\phi}(\mathbf{k})]_{12} - [H_{\phi\phi}(\mathbf{k})]_{21} \tag{B28}$$

$$B_A(\mathbf{k}) = \frac{2}{3}[\tilde{H}_{SS}(\mathbf{k})]_{11}$$

$$B_B(\mathbf{k}) = \frac{2}{3}[\tilde{H}_{SS}(\mathbf{k})]_{22}$$

$$B_{AB}(\mathbf{k}) = \frac{2}{3}[\tilde{H}_{SS}(\mathbf{k})]_{12} \tag{B29}$$

and

$$C_A(\mathbf{k}) = [H\phi_S(\mathbf{k})]_{11} - [H_{\phi S}(\mathbf{k})]_{21}$$

$$C_B(\mathbf{k}) = [H_{\phi S}(\mathbf{k})]_{12} - [H_{\phi S}(\mathbf{k})]_{22} \tag{B30}$$

References and Notes

(1) Bates, F. S.; Fredrickson, G. H. *Annu. Rev. Phys. Chem.* **1990**, *41*, 525.
(2) Bates, F. S.; Schulz, M. F.; Rosedale, J. H.; Almdal, K. *Macromolecules* **1992**, *25*, 5547.
(3) Liu, A. J.; Fredrickson, G. H. *Macromolecules* **1992**, *25*, 5551.
(4) Liu, A. J.; Fredrickson, G. H. *Macromolecules* **1993**, *26*, 2817.
(5) Helfand, E.; Sapse, A. M. *J. Chem. Phys.* **1975**, *62*, 1327.
(6) Liu, A. J.; Fredrickson, G. H. *Dynamics in Small Confining Systems*; Drake, J. M., Klafter, J., Kopelman, R., Awschalom, D. D., Eds.; *Mater. Res. Soc. Proc.* **1993**, *290*, 37.
(7) van Berkel, R. W. M.; de Graaf, S. A. F.; Huntjens, F. J.; Vrouenraets, C. M. F. *Developments in Block Copolymers—1*; Goodman, I., Ed.; Applied Science Publishers: New York, 1982; p 261.
(8) Krigbaum, W. R.; Zhang, S.-F.; Preston, J.; Ciferri, A.; Conio, G. *J. Polym. Sci., Part B* **1987**, *25*, 1043.
(9) Gottschalk, A.; Schmidt, H.-W. *Liq. Cryst.* **1980**, *5*, 1619.
(10) Enkelman, V.; Muller, W.; Wegner, G. *Synth. Met.* **1979/1980**, *1*, 185.
(11) Chien, J. C. W.; Wnek, G. E.; Karasz, F. E.; Hirsch, J. A. *Macromolecules* **1981**, *14*, 479.
(12) Baker, G. L.; Bates, F. S. *Macromolecules* **1984**, *17*, 2619.
(13) Stowell, J. A.; Amass, A. J.; Beevers, M. S.; Farren, T. R. *Polymer* **1989**, *30*, 195.
(14) Krouse, S. A.; Schrock, R. R. *Macromolecules* **1988**, *21*, 1885.
(15) Saunders, R. S.; Cohen, R. E.; Schrock, R. R. *Macromolecules* **1991**, *24*, 5599.
(16) Radzilowski, L. H.; Wu, J. L.; Stupp, S. I. *Macromolecules* **1993**, *26*, 879.
(17) Almdal, K.; Koppi, K. A.; Bates, F. S.; Mortensen, K. *Macromolecules* **1992**, *25*, 1743.
(18) Bates, F. S., private communication.
(19) Leibler, L. *Macromolecules* **1980**, *13*, 1602.
(20) Fredrickson, G. H.; Helfand, E. *J. Chem. Phys.* **1987**, *87*, 697.
(21) Helfand, E.; Wasserman, Z. R. *Macromolecules* **1976**, *9*, 879; **1978**, *11*, 961.
(22) Semenov, A. N. *Sov. Phys. JETP* **1985**, *61*, 733.
(23) Milner, S. T.; Witten, T. A.; Cates, M. E. *Europhys. Lett.* **1988**, *5*, 413; *Macromolecules* **1988**, *21*, 2610; *Macromolecules* **1989**, *22*, 853; *J. Phys. (Fr.)* **1988**, *19*, 1951.
(24) Ohta, T.; Kawasaki, K. *Macromolecules* **1986**, *19*, 2621.
(25) Vavasour, J. D.; Whitmore, M. D. *Macromolecules* **1992**, *25*, 5477.
(26) Fredrickson, G. H.; Leibler, L. *Macromolecules* **1990**, *23*, 531.
(27) Wang, X. J.; Warner, M. *Liq. Cryst.* **1992**, *12*, 385.
(28) Semenov, A. N.; Vasilenko, S. V. *Sov. Phys. JETP* **1986**, *63*, 70.
(29) Halperin, A. *Europhys. Lett.* **1989**, *10*, 549.
(30) Semenov, A. N. *Mol. Cryst. Liq. Cryst.* **1991**, *209*, 191.
(31) Williams, D. R. M.; Fredrickson, G. H. *Macromolecules* **1992**, *25*, 3561.
(32) Williams, D. R. M.; Halperin, A. *Phys. Rev. Lett.* **1993**, *71*, 1557.
(33) Holyst, R.; Schick, M. *J. Chem. Phys.* **1992**, *96*, 730.
(34) Holyst, R.; Schick, M. *J. Chem. Phys.* **1992**, *96*, 721.
(35) Fredrickson, G. H.; Leibler, L. *Macromolecules* **1990**, *23*, 531.
(36) We expect the incompressibility condition to work well in the weak segregation limit when at least one block is fairly flexible; it must break down, particularly in the interfacial region, when both blocks are stiff.
(37) Luckhurst, G. R.; Zannoni, C. *Nature* **1977**, *267*, 412.
(38) Since we have expanded the free energy to quadratic order in the order parameters, the isotropic–smectic and isotropic–nematic transitions both appear to be second order. If higher order terms terms in S_A and S_B are included, however, the isotropic–nematic transition becomes first order. Similarly, if higher order terms in ϕ are included, it is known from Leibler's work[19] that the isotropic–smectic transition becomes first order except at one value of f, where it is second order. For symmetric diblocks ($b_A = b_B$), the critical point is at $f = 0.5$. If fluctuations in ϕ are included, the critical point at $f = 0.5$ is replaced by a weakly first-order transition.[20] Thus, the isotropic–smectic transition is actually first order for all f. For this reason, we call the coexistence between isotropic, nematic, and smectic phases a triple point.
(39) Note that the isotropic–smectic and isotropic–nematic transitions are both second order within our quadratic approximation. Thus, the magnitudes of the order parameters are continuous at the transition, even though the value of k^* changes discontinuously at the transition.
(40) Bates, F. S.; Fredrickson, G. H., preprint. Fredrickson, G. H.; Liu, A. J.; Bates, F. S., preprint.
(41) Milner, S. T., unpublished.
(42) Ouimet, K.; Fredrickson, G. H., to be published.
(43) Morse, D. C.; Milner, S. T. *Phys. Rev. E* **1993**, *47*, 1119.
(44) Abramowitz, M.; Stegun, I. A., Eds. *Handbook of Mathematical Functions*; Dover Publications, Inc.: New York, 1972; p 231.